Overtone-Induced Chemistry of Trifluoroacetic Acid: An Experimental and Theoretical Study

Linda M. Reynard and D. J. Donaldson*

Scarborough College and Department of Chemistry, University of Toronto, 80 St. George Street, Toronto, Ontario, Canada M5S 3H6

Received: April 30, 2002; In Final Form: July 2, 2002

The effect of overtone-induced chemistry on the atmospheric fate of trifluoroacetic acid has been investigated. We report the absolute absorption intensities for the $\upsilon_{OH} = 3$, 4, and 5 overtone transitions as well as an ab initio calculation of the energetics of the dissociation pathways. Calculations at the MP2 level give the lowest dissociation barrier as 50.3 kcal mol^{-1} for the elimination of HF. Integrated cross sections for $\upsilon_{OH} = 3$, 4, and 5 are 2.70×10^{-20}, 1.68×10^{-21}, and 1.5×10^{-22} cm^2 molecule^{-1} cm^{-1}, respectively. Dissociation may proceed after absorption into $\upsilon = 5$ or 6, giving an upper limit to the photodissociation rate constants of 3.7×10^{-9} s^{-1} or 2.5×10^{-10} s^{-1}, respectively. These correspond to a tropospheric lifetime of between 8 and 127 years. The overtone-driven photodissociation is more important than the ultraviolet photodissociation in the troposphere but is insignificant in comparison to wet deposition and the reaction with OH radicals.

Introduction

The production and environmental fate of trifluoroacetic acid is not fully understood. Levels of trifluoroacetic acid predicted for the year 2010 on the basis of currently known sources have been reached already, suggesting that there are unknown sources of trifluoroacetic acid.[1,2] Known sources include the degradation products of hydrochlorofluorocarbons (HCFCs), hydrofluorocarbons (HFCs), and anesthetics.[2,3] The high-temperature use of fluorinated polymers has been suggested to be a significant additional source of trifluoroacetic acid.[4]

Models based on the projected use of HCFCs, HFCs, and anesthetics have been used to predict the amount of trifluoroacetic acid present in rainwater. Estimates of 89 ng L^{-1} (global average)[5] have been made for the year 2010, and 86 and 114 ng L^{-1} have been predicted for the year 2020.[3,6] However, trifluoroacetic acid has already reached the projected levels.

Levels of trifluoroacetate or trifluoroacetic acid in precipitation are reported to range from below the detection limit to 180 ng L^{-1} in various Canadian locations,[7] 33−220 ng L^{-1} in various sites in Switzerland,[8] 25−280 ng L^{-1} in Bayreuth, Germany,[9] and 7−136 ng L^{-1} (median concentrations) in California and Nevada.[10] In surface waters, such as lakes and rivers, concentrations of trifluoroacetic acid are in the range of <0.5−360 ng L^{-1} in Canadian lakes,[7] 60−280 ng L^{-1} in the Roter Main River in Germany,[9] and 45−433 ng L^{-1} in river and lake systems in California and Nevada.[10] These levels suggest that there is a major source of trifluoroacetic acid that is unknown and not accounted for in the models.

The cross section for ultraviolet photodissociation of trifluoroacetic acid has been measured and has been used to estimate a tropospheric lifetime of 1×10^5 years.[11] Two measurements have been made of the reaction rate with hydroxyl radicals, giving tropospheric lifetimes of 68 days[12] and 100 days.[13] The main sink for trifluoroacetic acid is wet deposition, contributing at least 75% of the total deposition.[6] This is estimated to occur with a rate similar that of to HNO_3, which has a washout time of approximately 9 days.[5,6] The overtone transitions of trifluoroacetic acid and their possible contribution to its photochemistry have not been studied.

Excitation of vibrational overtones can be important in atmospheric chemistry. In direct overtone photodissociation (DOP), overtone excitation is followed by energy transfer to a weaker bond, which may cause the molecule to dissociate. For example, pernitric acid is predicted to dissociate to $HO_2 + NO_2$ following excitation of the first overtone of the O−H stretch ($\upsilon_{OH} = 2$)[14] and has been observed experimentally to do so.[15] Because overtone transitions are less energetic and absorption cross sections are smaller than in the UV, most atmospheric photochemistry is driven by UV light. However, in cases where there is little UV light, for example, at high solar zenith angles or at the earth's surface, these weak overtone absorptions may become important. The DOP of pernitric acid has been calculated to be more important than UV photodissociation as a source of hydroxyl radicals at high solar zenith angles in the lower stratosphere.[16]

The purpose of this work is to investigate whether DOP might be important in the photochemistry of trifluoroacetic acid. Several dissociation pathways were calculated by ab initio methods to determine the lowest-energy channel, and the absorption spectra of the $\upsilon_{OH} = 3$, 4, and 5 overtones were measured to determine their positions and intensities. From these data, the photodissociation rate constant for DOP was estimated.

Computational Details

All calculations described here were performed with the Gaussian 98 suite of programs.[17] In most cases, second-order Møller−Plesset theory (MP2)[18] was used in conjunction with the 6-31G(d), 6-311G(d,p), and 6-311G(2d,p) basis sets provided by Gaussian 98.

The geometry of the structures was first optimized at the Hartree−Fock level of theory with the 6-31G(d) basis set, and the result were used as an initial structure for the MP2 calculations. In some cases, density functional theory (DFT)

* Corresponding author. E-mail: jdonalds@chem.utoronto.ca.

10.1021/jp021084w CCC: $22.00
Published on Web 08/27/2002

with a B3LYP functional[19] and the 6-311G(2d,p) basis set was used for comparison to the MP2 results. The transition states were found using the synchronous transit-guided quasi-Newton (STQN) method included in the Gaussian 98 program.[20] The result of this calculation was used for an optimization to a transition state. Harmonic frequencies and zero-point energies were calculated for all structures; the zero-point energies were used without correction. Stable molecules corresponding to a minimum on the potential energy surface were characterized by exclusively positive and real harmonic frequencies, whereas transition states all had a single imaginary frequency.

The transition states found were subjected to an intrinsic reaction coordinate calculation,[21,22] where the potential surface is followed in both directions away from the transition state and the geometry and energy are calculated at each point to verify that the transition state connects the reactant to the product.

Experimental Details

Apparatus. The apparatus used for overtone measurements is a 96.5-cm long Pyrex cell with quartz windows. The temperature of the cell is regulated by a water jacket connected to a circulating constant-temperature bath. A 468-W heating tape warms the region near the windows. The pressure in the cell is monitored with a capacitance manometer (Baratron 0-1000 Torr).

A 75-W Xe arc lamp is used as a light source. The light is collimated and passed through a UV blocking filter, which blocks wavelengths of less than 340 nm, and is directed through the cell. After passing through the cell, the light is focused by a lens (f/3) onto the entrance slit of a Czerny−Turner-type monochromator (CVI Laser) with a grating optimized for 750 nm. The entrance and exit slits are 0.15 mm wide, giving an effective resolution of 1 nm. Transmitted light is detected by a Si photodiode array (CVI Laser; detection range of 400−1100 nm) mounted at the exit slit of the monochromator. Its output is sent to a computer for analysis.

The trifluoroacetic acid used was 99+% pure, redistilled (Aldrich). Each sample was degassed by several freeze−pump−thaw cycles prior to use.

Data Analysis. Spectra were obtained in sets of five by averaging five background scans, filling the cell and averaging five scans, and using these two averages to calculate the absorbance, $A = -\ln(I/Io)$, at each wavelength. This process was repeated several times, and the resulting absorbances were averaged. Peak areas were calculated numerically using the trapezoid rule, giving the integrated absorbance, A_{int}. The integrated cross sections were determined from Beer's law, $A_{int} = \sigma_{int}Nl$, using the integrated absorbance at several different pressures.

Plots of the integrated absorbance versus total pressure are nonlinear and temperature-dependent because of the formation of dimers. To extract the monomer pressure, the equilibrium $M + M \rightleftharpoons D$, where M designates monomers and D, dimers, was considered. The equilibrium constant for dimerization, K, is given by

$$K = \frac{p_d}{p_m^2} \tag{1}$$

Combining eq 1 with $p_t = p_d + p_m$ results in an expression for the monomer pressure as a function of the equilibrium constant and the total pressure:

$$p_m = \frac{-1 + \sqrt{1 + 4Kp_t}}{2K} \tag{2}$$

To fit this expression to the available data of integrated absorbance as a function of total pressure, we assume that the integrated absorbance is proportional to the monomer pressure only. The monomer and dimer have infrared absorption maxima that do not overlap,[23] consistent with the dimer's calculated double hydrogen-bonded structure.[24,25] We anticipate that dimer overtone features will also be significantly red-shifted. In addition, the dependence of the dimer partial pressure on the total pressure is different from that given above for $p_{m.}$ For the monomer,

$$cA_{int} = p_m \tag{3}$$

where c is the proportionality constant. Substituting eq 3 into eq 2 gives an expression relating the integrated absorbance to the total pressure, the dimerization equilibrium constant, and the proportionality constant.

$$A_{int} = \frac{1 + \sqrt{1 + 4Kp_t}}{2Kc} \tag{4}$$

This expression was fit to the data, giving the dimerization equilibrium constant, K, and the proportionality constant, c. The equilibrium constant was used in eq 2 to determine the monomer pressure from the measured total pressure. Monomer number densities were derived from the monomer pressure by assuming ideal gas behavior. The integrated absorbance was plotted against the monomer number density times the path length; the integrated cross section is given by the slope of the line.

Results and Discussion

Calculations. Four dissociation channels of trifluoroacetic acid were considered.

$$CF_3COOH \rightarrow CF_2CO_2 + HF \tag{5}$$

$$CF_2CO_2 \rightarrow CO + COF_2 + HF \tag{5a}$$

$$CF_2CO_2 \rightarrow CO_2 + CF_2 + HF \tag{5b}$$

$$CF_3COOH \rightarrow CO_2 + CF_3H \tag{6}$$

$$CF_3COOH \rightarrow FCOOH + CF_2 \tag{7}$$

$$CF_3COOH \rightarrow HOCOCF_3 \tag{8}$$

Cleavage of the O−H bond has been calculated to require >100 kcal mol^{-1} [26] and was not considered in this work. Geometries, energies, and zero-point energy corrections were calculated for all species; the overall energetics are shown in Figure 1 and tabulated in Table 1. Optimized geometries and energies are given as Supporting Information.

The dissociation channel with the lowest energy barrier is the elimination of HF, which has a transition state 50.3 kcal mol^{-1} above the energy of trifluoroacetic acid. The second fragment forms a stable fluorinated epoxide, CF_2CO_2. The geometry of the HF-elimination transition state is given in Table 2 and is drawn in Figure 2a; the geometry of the epoxide intermediate is given in Table 3 and is illustrated in Figure 2b. This intermediate may dissociate either to CO + COF_2 or to CF_2 + CO_2, with transition states 6.5 and 18.4 kcal mol^{-1}, respectively, above the energy of the epoxide.

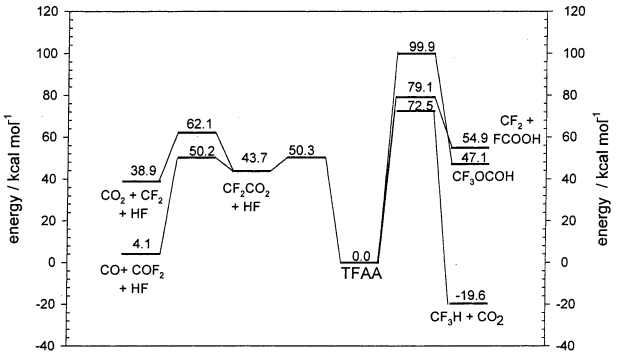

Figure 1. Calculated dissociation pathways at the MP2/6-311G(2d,p) level.

The other three channels considered here have higher-energy transition states: 72.5 kcal mol^{-1} for the decarboxylation (eq 6); 79.1 kcal mol^{-1} for the CF_2 elimination (eq 7); and 99.9 kcal mol^{-1} for the isomerization (eq 8). The latter two results compare well to a previous calculation at the MP4 level with a 6-31G(d) basis set;[26] however, the decarboxylation transition state reported here is almost 15 kcal mol^{-1} lower than the earlier result. The geometry we calculate has a C−C bond 0.2 Å shorter and an O−H bond 0.1 Å longer than the MP4/6-31G(d) result.[26]

Density functional theory results are given in Table 4 together with the MP2, MP4, and experimental results. The DFT and MP2 results are similar for the product energies of the decarboxylation channel (eq 6), but both are more negative than the experimental result by about 5 kcal mol^{-1}. For the product energies of the dissociation of the epoxide intermediate to CO_2 + CF_2 (eq 5b), the DFT and MP2 results agree but are about 4 kcal mol^{-1} lower than the experimental value. The DFT result (10.2 kcal mol^{-1}) is higher than both the MP2 (4.1 kcal mol^{-1}) and experimental (2.2 kcal mol^{-1}) results for the product energies of the dissociation of the epoxide to CO + COF_2 (eq 5a). The energy of the HF-elimination transition state calculated by the DFT method is lower than the MP2 result (45.9 vs 50.3 kcal mol^{-1}). Because neither method is variational,[27] it is not possible to give an upper limit to the true transition-state energy.

Many experimental studies have been made of the dissociation of trifluoroacetic acid. In particular, the dissociation has been effected by UV light,[12,28−30] multiple IR photons,[31] heat,[32−35] intermolecular energy transfer from SF_6,[36] and gamma radiation.[37,38] Products that have been identified include CO_2, C_2F_2, CO, CF_3H, H_2, CF_2, COF_2, CF_3COF, C_2F_4, SiF_4, $CF_3CO_2CF_2H$, and HF. In addition, some products have been inferred but not observed directly: CF_3, COOH, and F_2CCO_2.

The products observed in the various dissociation experiments are consistent with the calculated dissociation pathways of trifluoroacetic acid. No obvious differences were noted between the UV-induced dissociation products and ground-state dissociation products. The fluorinated epoxide proposed as an intermediate[39] has been calculated to be stable and a product of the lowest-energy dissociation channel.

The biradical F_2CCO_2 has been proposed as an intermediate following HF elimination from trifluoroacetic acid[31,36] and trifluoroacetic acid anhydride.[39] However, a direct decomposition to CF_2, HF, and CO_2 has also been proposed, the authors stating there is "no evidence to suggest the existence of the diradical CF_2CO_2".[34] Kubát and Pola suggest that the biradical is transformed to a second intermediate with a bridging oxygen between the two carbon atoms, giving a closed-valence molecule that dissociates into CO + COF_2.[39] Attempts to trap the biradical by hydrogen abstraction from ethane were unsuccessful.[39]

The energy of the biradical was not calculated here; it is expected to be higher in energy than the epoxide because it is an open-shell system. Kubát and Pola used a semiempirical method, MNDO, to calculate the energy and geometry of the fluorinated epoxide and the biradical.[39] The singlet biradical was calculated to be about 25 kcal mol^{-1} higher in energy than the epoxide, and the difference between the singlet and triplet biradicals is about 0.5 kcal mol^{-1}. The reaction energetics calculated using MNDO agree poorly with the MP2 results: the difference in energy between the epoxide and the products COF_2 + CO is 19 kcal mol^{-1} with the MNDO method and 39.6 kcal mol^{-1} for the MP2 calculation; for the products CF_2 + CO_2 the difference is 15 kcal mol^{-1} for the MNDO result and 4.8 kcal mol^{-1} for the MP2 result. Though agreement with ab initio results is quantitatively poor, the MNDO results agree qualitatively with the MP2 results with respect to the relative energies and indicate that the biradical is at a higher energy than the epoxide, as expected.

Activation energies have been extracted from a thermolysis experiment: 38.6 kcal mol^{-1} with respect to the loss of trifluoroacetic acid, 47.4 kcal mol^{-1} with respect to the appearance of CO_2, and 43.7 kcal mol^{-1} with respect to the appearance of CO.[32] The activation energy for the decarboxylation in water under 275 bars of pressure at temperatures over 100 °C is 46 kcal mol^{-1},[35] in agreement with the gas-phase result. The activation energies with respect to the appearance of CO_2 and CO are somewhat lower than the MP2 result for the HF-elimination channel (50.3 kcal mol^{-1}) and close to the DFT result (45.9 kcal mol^{-1}). The reasonable agreement of the experimental and calculated energy barriers supports the proposed mechanism of HF elimination followed by decomposition of CF_2CO_2.

Overtone Experiments. Figure 3 shows several spectra of the $\upsilon_{OH} = 3$ band of trifluoroacetic acid at several pressures. The area under each curve was measured, giving the integrated absorbance, A_{int}. In Figure 4, this is plotted against the total pressure for the two temperatures considered. The plot is nonlinear; fitting the data to eq 4 gives the dimerization equilibrium constant, K, of 25 ± 11 atm^{-1} at 333 K and 81 ± 40 atm^{-1} at 313 K (95% confidence level). This fit is shown by the dashed line in Figure 4. From these data, the thermodynamic parameters ΔH and ΔS may be obtained because

$$\ln K = \frac{-\Delta H}{RT} + \frac{\Delta S}{R} \qquad (9)$$

This gives $\Delta H = -51$ kJ mol^{-1} and $\Delta S = -125$ J mol^{-1} K^{-1}. These results are lower in absolute value than the literature values that fall in the range of −58.8 to −60.6 kJ mol^{-1} and −152 to −160.5 J mol^{-1}K^{-1} for ΔH and ΔS, respectively.[40−43] The thermodynamic parameters in this work were calculated with only two data points, so the results are not as precise as those from previous studies.

Because the thermodynamic parameters obtained from the fit agree poorly with the literature values, the average value of K from the four previous determinations was used to calculate the monomer pressure from eq 2 (16.6 ± 6 atm^{-1} at 333 K, 65.2 ± 21 atm^{-1} at 313 K; the limits given are twice the standard error of the mean).[40−43] These data are used with eq 4 to give the solid lines in Figure 4, which model the data well. The integrated absorbance is plotted versus monomer number density times path length in Figure 5. The data fall on a straight line, with a small positive intercept of the A_{int} axis. The slope gives the integrated cross section $\sigma_{int} = (2.70 \pm 0.09) \times 10^{-20}$ cm^2 molecule^{-1} cm^{-1}.

TABLE 1: MP2 Energies with Zero-Point Corrections (kcal mol^{-1})

	transition state			products		
	6-31G(d)	6-311G(d,p)	6-311G(2d,p)	6-31G(d)	6-311G(d,p)	6-311G(2d,p)
CF_3COOH						
$\rightarrow CF_2CO_2 + HF$	54.3	51.4	50.3	46.5	40.2	43.7
$\rightarrow CO_2 + CF_3H$	78.8	72.3	72.5	−19.9	−21.3	−19.6
$\rightarrow FCOOH + CF_2$	81.1	81.2	79.1	57.0	54.1	54.9
$\rightarrow HOCOCF_3$	100.5	100.6	99.9	47.1	46.2	47.1
$CF_2CO_2 + HF$						
$\rightarrow CO + COF_2 + HF$	55.2	48.3	50.2	11.1	0.4	4.1
$\rightarrow CO_2 + CF_2 + HF$	67.5	60.3	62.1	45.1	35.2	38.9

TABLE 2: Geometry and Energy of the HF-Elimination Transition State[a]

	6-31G(d)	6−312G(d,p)	6-311G(2d,p)
C−O	1.247	1.229	1.235
C−O′	1.245	1.240	1.239
C−C′	1.522	1.548	1.530
O′−H	1.571	1.468	1.497
C′−F	2.087	2.082	2.110
C′−F′	1.282	1.269	1.269
C′−F″	1.283	1.269	1.269
H−F	0.995	0.988	0.989
O−C−O′	139.5	139.2	138.9
O−C−C′	100.0	102.9	101.3
C−O′−H	96.6	97.3	96.5
C−C′−F	92.5	91.4	91.1
C−C′−F′	121.8	121.6	121.8
C−C′−F″	121.8	121.7	121.8
O−C−O′−H	180.0	−180.0	−180.0
O−C−C′−F	−180.0	180.0	180.0
O−C−C′−F′	−77.6	−77.5	−78.2
O−C−C′−F″	77.6	77.4	78.2
E	−525.39412	−525.69595	525.82027
ZPE	0.03508	0.03531	0.03529
E_{corr}	−525.35905	−525.66067	−525.78498

[a] Bond lengths in Å, bond angles in degrees, energies in hartrees.

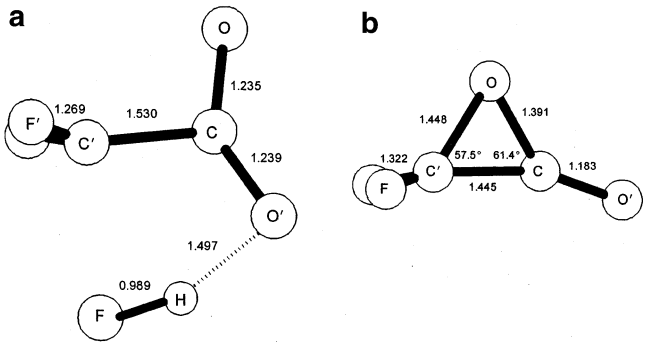

Figure 2. Geometries of intermediates calculated at the MP2/6-311G-(2d,p) level. (a) HF-elimination transition state. (b) CF_2CO_2.

Close examination of Figure 3 shows a small shoulder from 978 to 982 nm. The peak height of this shoulder as a function of total pressure is nonlinear but can also be fitted to eq 4, indicating that this feature is due to the monomer. As discussed above, dimer features display a different pressure dependence. We assign this feature to a combination band $2\upsilon_{OH} + 2\upsilon_{CO}$ Examination of the harmonic frequencies calculated from ab initio methods (Table 5) shows that $\upsilon_{OH} = 3$ falls at 886 nm and that the combination of $\upsilon_{OH} = 2$ and $\upsilon_{CO} = 2$ lies just 5 nm to the red at 891 nm ($2 \times (3764 + 1845)$ cm^{-1}), consistent with the experimental result. The C═O and O−H stretches do not differ in their degree of anharmonicity (2%),[44] so the relative positions predicted by the harmonic approximation should be correct.

Another possibility is an overtone plus bend, $(n - 1)\upsilon_{OH} + m\delta$. The highest-energy bend is the O−H in-plane at 1149 cm^{-1}

TABLE 3: Geometry and Energy of CF_2CO_2[a]

	6-31G(d)	6−312G(d,p)	6-311G(2d,p)
C−O	1.390	1.381	1.391
C−O′	1.195	1.184	1.183
C′−O	1.448	1.439	1.448
C−C′	1.444	1.445	1.445
C′−F	1.332	1.322	1.322
C′−F′	1.331	1.322	1.322
O−C−O′	138.5	138.4	138.4
O−C−C′	61.4	61.2	61.4
O−C′−C	57.5	57.2	57.5
C−C′−F	115.1	123.9	123.7
C−C′−F′	115.1	123.9	123.7
O′−C−C′−O	179.9	180.0	179.9
O−C−C′−F	−100.3	−99.9	−100.2
O−C−C′−F′	100.3	99.9	100.2
E	−425.22169	−425.44437	−425.53988
ZPE	0.02325	0.02330	0.02291
E_{corr}	−425.19844	−425.42106	−425.51696

[a] Bond lengths in Å, bond angles in degrees, energies in hartrees.

(assigned by reference to the infrared spectrum).[23] In this case, a peak is predicted at 10 975 cm^{-1} ($2 \times 3764 + 3 \times 1149$ cm^{-1}). This is in the correct relative position but lies 25 nm from the $\upsilon_{OH} = 3$ peak. All other bends are low frequency (<806 cm^{-1}) and can be eliminated from consideration.

Therefore, the most plausible assignment for the shoulder is the $2\upsilon_{OH} + 2\upsilon_{CO}$ combination band. Because the C═O and O−H are just one bond away from each other, it is not surprising that their stretches might be coupled to each other.

The $\upsilon_{OH} = 4$ overtone is seen in the region 735−765 nm and is illustrated in Figure 6a. The only peak in this spectral region is located at 749.0 nm; it is assigned to the $\upsilon_{OH} = 4$ overtone. The intensity is much lower than the $\upsilon_{OH} = 3$ overtone; as a result, spectra were acquired only at 333 K because at lower temperatures the monomer number density is lower, thus decreasing the peak intensity and making the spectrum acquisition more difficult.

The plot of integrated absorbance against total pressure is again nonlinear. The monomer pressure was calculated as before, and the integrated absorbance was plotted against monomer number density times path length. The result is shown in Figure 6b: the points fall on a straight line, with a small positive intercept of the ordinate. The slope of the regression line gives an integrated cross section of $(1.68 \pm 0.19) \times 10^{-21}$ cm^2 molecule^{-1} cm^{-1}. This overtone is 16 times weaker than the $\upsilon_{OH} = 3$ overtone.

Using the peak wavelengths of the two overtone bands and the fundamental,[23] the Morse parameters for the O−H stretch of trifluoroacetic acid were calculated from

$$\Delta G_{0-\upsilon} = \upsilon\omega_e - \upsilon(\upsilon + 1)\omega_e x_e \qquad (10)$$

to obtain $\omega_e = 3749 \pm 10$ cm^{-1} and $\omega_e x_e = 82 \pm 2$ cm^{-1}. These Morse parameters are compared to those of other O−H stretch overtones in Table 6.

TABLE 4: Energies with Zero-Point Corrections (kcal mol^{-1}); 6-311G(2d,p) Basis Set

	transition state			products			
	MP2	B3LYP	MP4[a]	MP2	B3LYP	MP4[a]	expt[b]
CF_3COOH							
$\rightarrow CF_2CO_2 + HF$	50.3	45.9		43.7	45.3		
$\rightarrow CO_2 + CF_3H$	72.5		87.3	−19.6	−18.9	−16.6	−14.2
$\rightarrow FCOOH + CF_2$	79.1		81.6	54.9		52.4	
$\rightarrow HOCOCF_3$	99.9		104.2	47.1		44.0	
$CF_2CO_2 + HF$							
$\rightarrow CO + COF_2 + HF$	50.2			4.1	10.2		2.2
$\rightarrow CO_2 + CF_2 + HF$	62.1			38.9	39.2		43.9

[a] 6-31G(d) basis set, ref 26. [b] References 49 and 50.

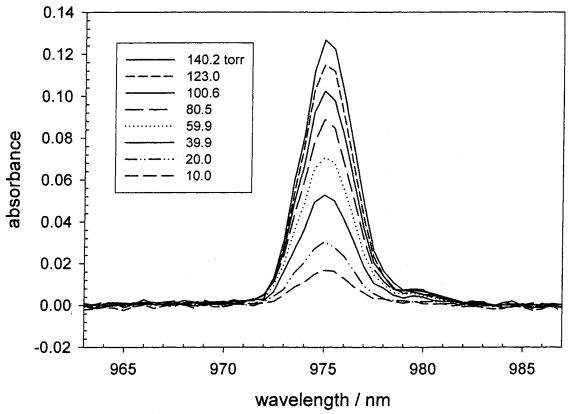

Figure 3. Absorption spectrum of the $\upsilon_{OH} = 3$ overtone of trifluoroacetic acid at 333 K measured at various total pressures.

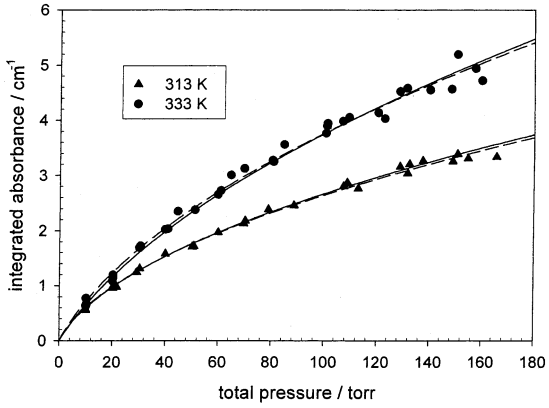

Figure 4. Integrated absorbance vs total pressure for the $\upsilon_{OH} = 3$ overtone of trifluoroacetic acid at 333 K (●) and 313 K (▲). Dashed lines are fits to eq 2. Solid lines are plots of eq 2 using the literature values of *K*.

Using these Morse parameters, a prediction for the position of the $\upsilon_{OH} = 5$ overtone of 614 nm is obtained. Because the overtone was expected to be weak, 640 spectra, acquired in groups of 5, were averaged. This resulted in a small peak on a sloping baseline. The baseline was corrected by drawing a line through the apparent baseline and setting it to zero, and the resulting spectrum is shown in Figure 7.

With just a single data point, the integrated cross section was obtained directly from Beer's law. Two integration areas (5- and 3-nm wide) were used to obtain two estimates for the cross section because of uncertainty in determining the peak width because of the low signal-to-noise ratio. This gives integrated cross sections, σ_{int}, of 1.79×10^{-22} cm^2 molecule^{-1} cm^{-1} and 1.13×10^{-22} cm^2 molecule^{-1} cm^{-1}, respectively. The integrated absorption cross section is therefore estimated to be $\sim 1.5 \times 10^{-22}$ cm^2 molecule^{-1} cm^{-1}. Because of the low signal-to-noise ratio, the direct use of Beer's law, and the baseline correction,

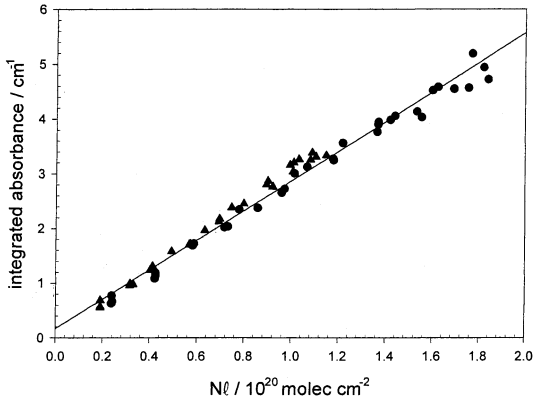

Figure 5. Integrated absorbance vs (monomer number density × path length) for the $\upsilon_{OH} = 3$ overtone of trifluoroacetic acid at 333 K (●) and 313 K (▲). The slope of the regression line gives the integrated cross section, σ_{int}.

TABLE 5: MP2/6-311G(2d,p) Harmonic Frequencies (cm^{-1}) for CF_3COOH

37.4	242.5	248.3	396.5	431.2
512.1	595.1	618.8	672.7	796.8
805.6	1148.7	1218.9	1241.3	1290.6
1458.5	1845.5	3764.0		

this measurement of the cross section is much less precise than that of the $\upsilon_{OH} = 3$ and 4 bands.

The integrated cross sections of the $\upsilon_{OH} = 3$ overtones of methanol and acetic acid were also measured for comparison to previous results. Because acetic acid also forms dimers, the dimerization equilibrium constant is needed. $\Delta H = -61.0$ kJ mol^{-1} and $\Delta S = -145.5$ J mol^{-1} K^{-1} were used to calculate *K* at 333 K ($K = 93.0$ atm^{-1}).[45]

The integrated cross sections are given in Table 7 in addition to some previous results. The result for acetic acid and methanol agree with the earlier determinations. The integrated cross section of trifluoroacetic acid decreases by a factor of 16 from $\upsilon = 3$ to 4 and by approximately a factor of 10 from $\upsilon = 4$ to 5. The cross section for $\upsilon = 3$ of trifluoroacetic acid is lower than that of acetic acid by a factor of 1.2; fluorination decreases the cross section of ethanol by the same factor. These results indicate that the intensity of the overtones of the O−H stretch changes according to the chemical environment.

Photodissociation Rate Constant. Using the result of the ab initio calculation of the energy barrier to dissociation and the overtone intensities, the atmospheric photodissociation rate was estimated. The photodissociation rate constant, *J*, is given by

$$J = \int_{\lambda} I(\lambda)\, \sigma(\lambda)\, \phi(\lambda)\, d\lambda \qquad (11)$$

where $I(\lambda)$ is the actinic flux, $\sigma(\lambda)$ is the absorption cross section,

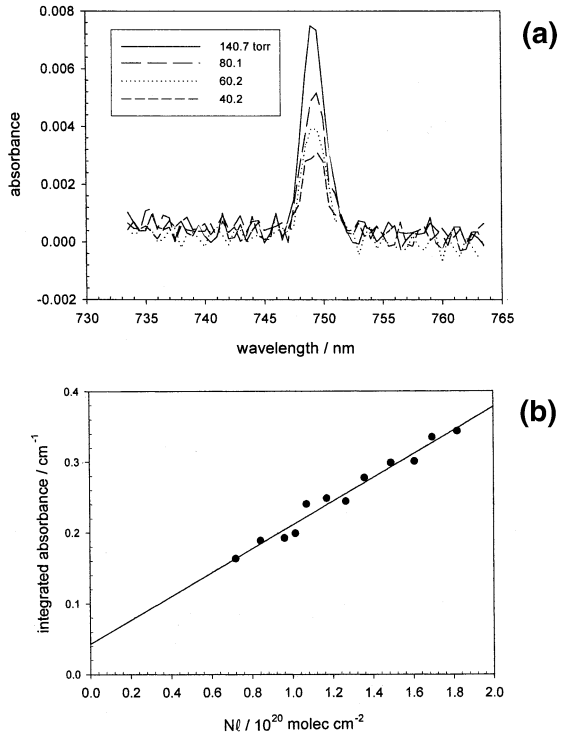

Figure 6. $\upsilon_{OH} = 4$ overtone of trifluoroacetic acid at 333 K. (a) Absorption spectrum measured at various total pressures. (b) Integrated absorbance vs (monomer number density × path length).

TABLE 6: Morse Potential Parameters (cm^{-1})[a]

	ω_e	$\omega_e x_e$	reference
methanol	3856(12)	86(3)	51
	3853(13)	85(3)	52
ethanol	3845(17)	87(4)	51
	3836(15)	85(5)	52
trifluoroethanol	3826(13)	84(3)	52
acetic acid	3747(19)	83(7)	52
trifluoroacetic acid	3749(10)[b]	82(2)[b]	this work

[a] Numbers in parentheses are error limits in units of the last digit. [b] Error limits are two standard deviations of the slope of the regression line.

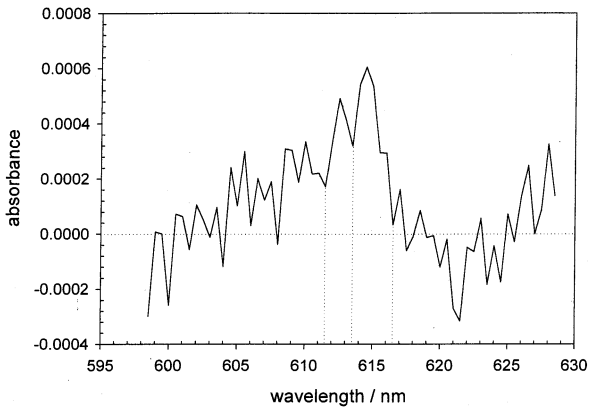

Figure 7. Absorption spectrum of the $\upsilon_{OH} = 5$ overtone of trifluoroacetic acid at 333 K and ~140 Torr total pressure after baseline correction. The dotted lines show the two integration areas.

and $\phi(\lambda)$ is the quantum yield. Each of these quantities is wavelength-dependent, and the integration is made over the wavelengths of interest.

According to the MP2 ab initio calculations, the lowest energy barrier is for HF elimination at 50.3 kcal mol^{-1}, corresponding to a wavelength <569 nm. This is accessible following excitation to the $\upsilon_{OH} = 6$ overtone, which is predicted to lie at 525 nm. The cross section for this overtone has not been determined. However, given that we estimate σ_{int} for the $\upsilon_{OH} = 5$ overtone to be 1.5×10^{-22} cm^2 $molecule^{-1}$ cm^{-1} and assuming a decrease of a factor of 10 per additional quantum of stretch, an integrated cross section of 1.5×10^{-23} cm^2 $molecule^{-1}$ cm^{-1} is a reasonable guess for the intensity of the $\upsilon_{OH} = 6$ overtone.

TABLE 7: Integrated Cross Section (cm^2 $molecule^{-1}$ cm^{-1})[a]

	$\upsilon = 3$ ($\times 10^{-20}$)	$\upsilon = 4$ ($\times 10^{-21}$)	$\upsilon = 5$ ($\times 10^{-22}$)	reference
methanol	2.46(18)[b]			this work
	2.10(21)	2.25(25)	3.50(35)	51
	2.40(15)	1.69(14)		52
ethanol	2.37(24)	2.37(24)		51
	2.24(13)	1.52(19)		52
trifluoroethanol	1.83(11)	1.26(10)		52
acetic acid	3.21(89)[b]			this work
	3.10(45)			52
trifluoroacetic acid	2.70(9)[b]	1.68(19)[b]	~1.5	this work

[a] Numbers in parentheses are error limits in units of the last digit. [b] Error limits are two standard deviations of the slope of the regression line.

TABLE 8: Photodissociation Rate Constant, J (s^{-1})

altitude (km)	$DOP_{\upsilon=6}$	$DOP_{\upsilon=5}$	UV
0	2.5×10^{-10}	3.7×10^{-9}	0
15	2.7×10^{-10}	3.8×10^{-9}	
20			6.7×10^{-9}
25	2.7×10^{-10}	3.8×10^{-9}	
30			5.0×10^{-7}
40	2.7×10^{-10}	3.8×10^{-9}	3.7×10^{-6}
50			9.7×10^{-6}

Actinic fluxes for solar zenith angle of 30° were taken from ref 46. The HF quantum yield is assumed to be unity because the overtone transition lies above the dissociation threshold. Using these parameters gives a value of $J = 2.5 \times 10^{-10}$ s^{-1} at 0 km and $J = 2.7 \times 10^{-10}$ s^{-1} at altitudes >15 km, corresponding to a lifetime of 127 or 117 years, respectively. These values of J represent an upper limit to the photodissociation rate constant because the quantum yield is unknown.

The DFT energy of the HF-elimination transition state is 4.4 kcal mol^{-1} lower than the MP2 result. This energy corresponds to a wavelength >623 nm, suggesting that the $\upsilon_{OH} = 5$ overtone could effect the dissociation. The actinic fluxes in this wavelength range are slightly higher than at 525 nm,[46] giving a photodissociation rate constant of more than an order of magnitude larger: $J = 3.7 \times 10^{-9}$ s^{-1} at 0 km and $J = 3.8 \times 10^{-9}$ s^{-1} at the other altitudes. This gives a tropospheric lifetime of 8 years.

The J value was also calculated for the ultraviolet photodissociation of trifluoroacetic acid. The wavelength-dependent actinic fluxes for altitudes of 0−50 km were used (solar zenith angle 30°, assuming U. S. Standard Atmosphere (1976), surface albedo 0.3),[47] along with the absorption cross section in the range 200−280 nm.[48] The resulting J values are given in Table 8, along with the results of the DOP estimates.

Because the cross section is the main uncertainty in this calculation, J was calculated with a cross section for absorption to $\upsilon_{OH} = 6$ that differs from the estimate by a factor of 2. An integrated cross section of 3×10^{-23} cm^2 $molecule^{-1}$ cm^{-1} gives $J = 4.9 \times 10^{-10}$ s^{-1} at 0 km, whereas an integrated cross section of 7.5×10^{-24} cm^2 $molecule^{-1}$ cm^{-1} gives $J = 1.2 \times 10^{-10}$ s^{-1} at 0 km. These results give lifetimes of 65 and 264 years, respectively.

At the earth's surface, the dissociation by DOP is dominant over UV photodissociation. The photodissociation rate coefficient for DOP remains constant at altitudes greater than 15 km because there is little attenuation of visible light. The UV photodissociation becomes increasingly important at higher altitudes because more UV light is available. At 50 km, for example, this results in a photodissociation lifetime of 29 h.

Whereas DOP is more important than UV photodissociation at the surface, it is not competitive with wet deposition (lifetime ~9 days)[5,6] or reaction with OH radicals (lifetime ~68−100 days).[12,13]

Conclusions

The dissociation pathways for trifluoroacetic acid were calculated with ab initio methods at the MP2 level of theory, giving the lowest dissociation barrier of 50.3 kcal mol^{-1} for the elimination of HF. The DFT result is lower at 45.9 kcal mol^{-1}. The $\upsilon_{OH} = 3$, 4, and 5 overtones were measured. The photodissociation rate constant for direct overtone photodissociation was estimated, giving $J = 3.7 \times 10^{-9}$ s^{-1} for the lower DFT dissociation barrier and $J = 2.5 \times 10^{-10}$ s^{-1} for the higher MP2 barrier, corresponding to a tropospheric lifetime of approximately 8 or 127 years, respectively. This process is much more important than the tropospheric UV photodissociation but is insignificant in comparison to wet deposition and the reaction with OH radicals.

Acknowledgment. This work was funded by the Natural Science and Engineering Research Council of Canada. L.M.R. thanks NSERC for a postgraduate scholarship.

Supporting Information Available: The geometries and energies of CF_3COOH, CO, CO_2, CF_3H, CF_2, FCOOH, COF_2, $HOCOCF_3$, and HF and of the transition state of reactions 5a, 5b, 6, 7, and 8. This material is available free of charge via the Internet at http://pubs.acs.org.

References and Notes

(1) Jordan, A.; Frank, H. *Environ. Sci. Technol*. **1999**, *33*, 522.
(2) Boutonnet, J. C.; Bingham, P.; Calamari, D.; de Rooij, C.; Franklin, J.; Kawano, T.; Libre, J.-M.; McCulloch, A.; Malinverno, G.; Odom, J. M.; Rusch, G. M.; Smythe, K.; Sobolev, I.; Thompson, R.; Tiedje, J. M. *Hum. Ecol. Risk Assess*. **1999**, *5*, 59.
(3) Tang, X.; Madronich, S.; Wallington, T.; Calamari, D. *J. Photochem. Photobiol., B* **1998**, *46*, 83.
(4) Ellis, D. A.; Mabury, S. A.; Martin, J. W.; Muir, D. C. G. *Nature (London)* **2001**, *412*, 321.
(5) Kotamarthi, V. R.; Rodriguez, J. M.; Ko, M. K. W.; Tromp, T. K.; Sze, N. D.; Prather, M. J. *J. Geophys. Res., D: Atmos.* **1998**, *103*, 5747.
(6) Kanakidou, M.; Dentener, F. J.; Crutzen, P. J. *J. Geophys. Res., D: Atmos*. **1995**, *100*, 18781.
(7) Scott, B. F.; Mactavish, D.; Spencer, C.; Strachan, W. M. J.; Muir, D. C. G. *Environ. Sci. Technol*. **2000**, *34*, 4266.
(8) Berg, M.; Muller, S. R.; Muhlemann, J.; Wiedmer, A.; Schwarzenbach, R. P. *Environ. Sci. Technol.* **2000**, *34*, 2675.
(9) Frank, H.; Klein, A.; Renschen, D. *Nature (London)* **1996**, *382*, 34.
(10) Wujcik, C. E.; Cahill, T. M.; Seiber, J. N. *Environ. Sci. Technol.* **1999**, *33*, 1747.
(11) Wild, O.; Rattigan, O. V.; Jones, R. L.; Pyle, J. A.; Cox, R. A. *J. Atmos. Chem*. **1996**, *25*, 167.
(12) Møgelberg, T. E.; Nielsen, O. J.; Sehested, J.; Wallington, T. J.; Hurley, M. D. *Chem. Phys. Lett*. **1994**, *226*, 171.
(13) Carr, S.; Treacy, J. J.; Sidebottom, H. W.; Connell, R. K.; Canosa-Mas, C. E.; Wayne, R. P.; Franklin, J. *Chem. Phys. Lett.* **1994**, *227*, 39.
(14) Staikova, M.; Donaldson, D. J.; Francisco, J. S. *J. Phys. Chem. A* **2002**, *106*, 3023.
(15) Roehl, C. M.; Nizkorodov, S. A.; Zhang, H.; Blake, G. A.; Wennberg, P. O. *J. Phys. Chem. A*, in press.
(16) Donaldson, D. J.; Tuck, A. F., Vaida, V. *Phys. Chem. Earth, Part C* **2000**, *25*, 223.
(17) Frisch, M. J.; Trucks, G. W.; Schlegel, H. B.; Scuseria, G. E.; Robb, M. A.; Cheeseman, J. R.; Zakrzewski, V. G.; Montgomery, J. A., Jr.; Stratmann, R. E.; Burant, J. C.; Dapprich, S.; Millam, J. M.; Daniels, A. D.; Kudin, K. N.; Strain, M. C.; Farkas, O.; Tomasi, J.; Barone, V.; Cossi, M.; Cammi, R.; Mennucci, B.; Pomelli, C.; Adamo, C.; Clifford, S.; Ochterski, J.; Petersson, G. A.; Ayala, P. Y.; Cui, Q.; Morokuma, K.; Malick, D. K.; Rabuck, A. D.; Raghavachari, K.; Foresman, J. B.; Cioslowski, J.; Ortiz, J. V.; Stefanov, B. B.; Liu, G.; Liashenko, A.; Piskorz, P.; Komaromi, I.; Gomperts, R.; Martin, R. L.; Fox, D. J.; Keith, T.; Al-Laham, M. A.; Peng, C. Y.; Nanayakkara, A.; Gonzalez, C.; Challacombe, M.; Gill, P. M. W.; Johnson, B. G.; Chen, W.; Wong, M. W.; Andres, J. L.; Head-Gordon, M.; Replogle, E. S.; Pople, J. A. *Gaussian 98*, revision A.7; Gaussian, Inc.: Pittsburgh, PA, 1998.
(18) Møller, C.; Plesset, M. S. *Phys. Rev.* **1934**, *46*, 618.
(19) Becke, A. D. *J. Chem. Phys.* **1993**, *98*, 5648.
(20) Peng, C.; Ayala, P. Y.; Schlegel, H. B.; Frisch, M. J. *J. Comput. Chem.* **1998**, *17*, 49. Peng, C.; Schlegel, H. B. *Isr. J. Chem.* **1994**, *33*, 449.
(21) Gonzalez, C.; Schlegel, H. B. *J. Chem. Phys.* **1989**, *90*, 2154.
(22) Gonzalez, C.; Schlegel, H. B. *J. Phys. Chem.* **1990**, *94*, 5523.
(23) Kagarise, R. E. *J. Chem. Phys.* **1957**, *27*, 519.
(24) Szàsz, G.; Borisenko, K. B.; Hargittai, I. *J. Mol. Struct.: THEOCHEM* **1997**, *393*, 111.
(25) Frurip, D. J.; Curtiss, L. A.; Blander, M. *J. Am. Chem. Soc.* **1980**, *102*, 2610.
(26) Francisco, J. S. *J. Chem. Soc., Faraday Trans.* **1992**, *88*, 3521.
(27) Levine, I. N. *Quantum Chemistry*, 5th ed.; Prentice Hall: Upper Saddle River, NJ, 2000; p 566.
(28) Mearns, A. M.; Back, R. A. *Can. J. Chem.* **1963**, *41*, 1197.
(29) Osborne, M. C.; Li, Q.; Smith, I. W. M. *Phys. Chem. Chem. Phys.* **1999**, *1*, 1447.
(30) Kwon, H. T.; Shin, S. K.; Kim, S. K.; Kim, H. L.; Park, C. R. *J. Phys. Chem. A* **2001**, *105*, 6775.
(31) Kumar, A.; Vatsa, R. K.; Naik, P. D.; Rama Rao, K. V. S.; Mittal, J. P. *Chem. Phys. Lett.* **1993,** *208*, 385.
(32) Blake, P. G.; Pritchard, H. *J. Chem. Soc. B* **1967**, 282.
(33) Ashworth, A.; Harrison, P. G. *J. Chem. Soc., Faraday Trans.* **1993**, *89*, 2409.
(34) Jollie, D. M.; Harrison, P. G. *J. Chem. Soc., Perkin Trans.*, **1997**, *2*, 1571.
(35) Belsky, A. J.; Maiella, P. G.; Brill, T. B. *J. Phys. Chem. A* **1999**, *103*, 4253.
(36) Pola, J. *Collect. Czech. Chem. Commun.* **1981**, *46*, 2854.
(37) Betts, J.; Cherniak, E. A. *Can. J. Chem.* **1971**, *49*, 3389.
(38) Ayscough, P. B.; Mach, K. *J. Chem. Soc., Faraday Trans.* **1974**, *70*, 118.
(39) Kubát, P.; Pola, J. *Collect. Czech. Chem. Commun*. **1990**, *55*, 2460.
(40) Lumbroso-Bader, N.; Coupry, C.; Baron, D.; Clague, D. H. *J. Magn. Reson.* **1975**, *17*, 386.
(41) Sauren, H.; Winkler, A.; Hess, P. *Chem. Phys. Lett.* **1995**, *239*, 313.
(42) Taylor, M. D.; Templeman, M. B. *J. Am. Chem. Soc*. **1956**, *78*, 2950.
(43) Lundin, R. E.; Harris, F. E.; Nash, L. K. *J. Am. Chem. Soc*. **1952**, *74*, 4654.
(44) Huber, K.-P.; Herzberg, G. *Molecular Spectra and Molecular Structure*; Van Nostrand Reinhold: New York, 1979; Vol. 4.
(45) Clague, A. D. H.; Bernstein, H. J. *Spectrochim. Acta, Part A* **1969**, *25*, 593.
(46) Madronich, S.; Finlayson-Pitts, B. J.; Pitts, J. N., Jr. In *Chemistry of the Upper and Lower Atmosphere: Theory, Experiments and Applications*; Academic Press: London, 2000.
(47) DeMore, W. B.; Sander, S. P.; Golden, D. M.; Hampson, R. F.; Kurylo, M. J.; Howard, C. J.; Ravishankara, A. R.; Kolb, C. E.; Molina, M. J. *JPL Publication 97-4*, 1997.
(48) Rattigan, O. V.; Wild, O.; Jones, R. L.; Cox, R. A. *J. Photochem. Photobiol., A* **1993**, *73*, 1.
(49) Chase, M. W., Jr. NIST−JANAF Themochemical Tables, 4th ed. *J. Phys. Chem. Ref. Data;* ACS Monograph 9, American Chemical Society: Washington, DC, 1998; p 1.
(50) Pedley, J. B.; Naylor, R. D.; Kirby, S. P. *Thermochemical Data of Organic Compounds*; Chapman and Hall: New York, 1986.
(51) Phillips, J. A.; Orlando, J. J.; Tyndall, G. S.; Vaida, V. *Chem. Phys. Lett*. **1998**, *296*, 377.
(52) Lange, K. R.; Wells, N. P.; Plegge, K. S.; Phillips, J. A. *J. Phys. Chem. A* **2001**, *105*, 3481.
(53) Antolinez, A.; Alonso, J. L.; Dreizler, H.; Hentrop, E.; Sutter, D. H. *Z. Naturforsch., A: Phys. Sci.* **1999**, *54*, 524.